Classification of cracking mode in concrete by acoustic emission parameters

Dimitrios G. Aggelis *

Department of Materials Science and Engineering, University of Ioannina, 45110 Ioannina, Greece

ARTICLE INFO

ABSTRACT

The study occupies with acoustic emission monitoring of several types of concrete during bending. The signals emitted at the different fracturing stages exhibit distinct signatures. Specifically, frequency and shape parameters of the acquired waveforms shift during the experiment, closely following the sequence of fracture mechanisms from tensile micro-cracking to brittle macro-cracking and fiber pull out. A number of AE indices are proposed, the use of which will enable classification of the cracks according to their mode. The study sheds light to the fracture process of cementitious materials, and enables a warning against the final failure. The simplicity of the scheme renders it applicable in situ.

© 2011 Elsevier Ltd. All rights reserved.

1. Introduction

The importance of monitoring of the structural safety of concrete structures has been long stated. Early assessment of material condition against large-scale failure helps to manage the structures safely and economically. One of the methods used for real time nondestructive monitoring is acoustic emission (AE). Using this technique, the elastic waves released during crack propagation incidences are recorded by transducers placed on the surface of the material (Grosse and Ohtsu, 2008; Mindess, 2004). The transducers are usually piezoelectric and transform the energy of the transient elastic wave to an electric waveform which is digitized and stored. The information of these waveforms includes the location of the source crack (by comparing the arrival time to different sensors), the density of cracks, as well as the severity of the materials condition (Kurz et al., 2006; Aggelis et al., 2010a; Carpinteri et al., 2010; Matikas, 2008; Zhou et al., 2010). A very important aspect is the correlation of AE indices to the cracking mode. For most cases of materials and loadings until failure, tensile cracks are developed at the initial stage of loading, while shear cracks dominate later (Yuyama et al., 1999). This is typical for reinforced concrete members that undergo bending. The initial cracking comes from the tensile load on the surface of concrete, while the member ultimately fails with diagonal shear cracks (Ohno and Ohtsu, 2010). Therefore, it is beneficial to characterize the mode of the cracks as it can lead to early assessment of the materials condition. For this goal, Moment Tensor Analysis (MTA) provides information taking into account the first cycle of each AE signal. The results have been demonstrated in laboratory conditions in various experiments suc-

cessfully classifying the cracks depending on their mode (Ohno and Ohtsu, 2010; Kawasaki et al., 2010). However, in certain cases of structures the application is not straightforward mainly because of the number of necessary sensors to detect each cracking event (at least six). The crack location is not known a priori, and therefore the sensors are distributed evenly to cover the largest amount of material volume. Thus, the distance between neighboring sensors does not allow capturing one single cracking event by the necessary number of sensors. Especially in long structures like bridges, the sensors are placed in a straight line in order to cover as much as possible of the structure's dimension (Shiotani et al., 2009). This placement enables only linear location of the damage zones but is not suitable for MTA. Therefore, simple characterization schemes are sought for, which would enable characterization of the cracking mode based on the information of a small number of sensors.

It has been seen that a crack propagation incidence has different acoustic emission signatures depending on the mode of the crack. The tensile mode of crack which includes opposing movement of the crack sides, results in AE waveforms with short rise time and high frequency. On the contrary shear type of cracks usually result in longer waveforms, with lower frequency and longer rise time (Aggelis et al., 2010b). This is mainly due to the larger part of energy transmitted in the form of shear waves, which are slower; therefore, the maximum peak of the waveform delays considerably compared to the onset of the initial longitudinal arrivals. This has been demonstrated in different kinds of materials, like concrete (Ohno and Ohtsu, 2010; Soulioti et al., 2009), fiber composites (Philippidis et al., 1998; Aggelis et al., 2010c) and rock (Shiotani, 2006). Fig. 1 shows a typical AE signal after a crack propagation event with its main features. One of the crucial parameters which are influenced by the mode of crack according to the above discussion is the average frequency, AF which is defined by the ratio of threshold crossings over the duration of the signal and is measured

* Tel.: +30 26510 08006; fax: +30 26510 08054.
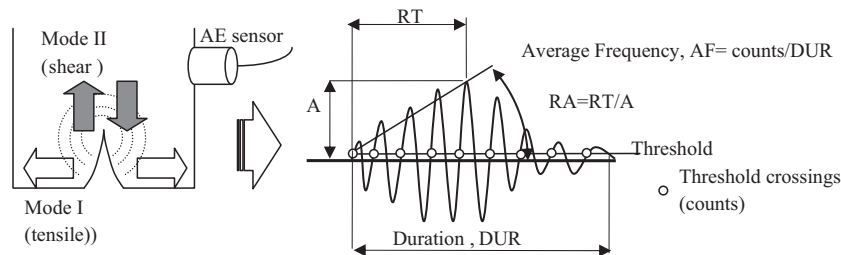 *E-mail address:* daggelis@cc.uoi.gr

Fig. 1. Crack modes and AE signal.

in kHz. It is one estimate of the basic frequency content of the waveform. Another crucial parameter is the RA value which is the rise time (RT, delay between the onset and the maximum amplitude) over the amplitude, A, measured in $\mu s/V$. AE energy (ENE) is another important parameter expressing the measure of the area under the rectified signal envelope (MARSE). It is reasonable to suggest that the energy in the acoustic waveform is proportional to the energy of the associated deformation (Curtis, 1975) and is presented in dimensionless form (Philippidis et al., 1999). It expresses the severity of an event since large crack propagation incidences will emit larger amount of energy than micro-cracks. These parameters have been used to characterize the cracking mode in laboratory conditions in accelerated corrosion experiments in reinforced concrete (Ohtsu and Tomoda, 2007), in bending of concrete reinforced with metal bars (Ohno and Ohtsu, 2010), with steel fibers (Soulioti et al., 2009) as well as vinyl fibers (Aggelis et al., 2009). The results have shown that the emissions during the early damage stage (corresponding to tensile mode) exhibit higher AF and lower RA, while as the material is led to final failure AF decreases and RA increases. Based on above studies, it can be concluded that tensile matrix cracking results in AF higher than approximately 300 kHz and RA lower than 500 $\mu s/V$ as measured by broadband transducers (Aggelis et al., 2010d). When sensors of low resonant frequency (nominally 150 kHz) are used the values 60 kHz and 2000 $\mu s/V$ are suggested for AF and RA respectively (Soulioti et al., 2009). It would be desirable to test the above conclusions over a wide variety of concrete materials in order to estimate if the validity of any such criteria is global, or if they should be used in a case-specific basis, depending on the type of the material. This is of paramount importance in the field of engineering, while it is the subject of relevant scientific committees aiming at standardization of the AE testing in the concrete field (Ohtsu, 2010).

The shape of the AE signal apart from its origin is influenced by other conditions. One is scattering while propagating, which results from the inherent inhomogeneity of concrete due to its microstructure (sand, gravels, air voids, pores as well as cracking). Another influence comes from the differential velocity of the distinct wave modes excited by the source crack, as well as the mode conversion on the surface. This is inevitable since in AE testing the signal is acquired from the surface and is certain to include all different wave modes, including Rayleigh waves after impinging on the surface. Since the velocities of the modes are different, the waveform will be continuously spreading in time and the actual shape recorded will depend on the location of the sensor relatively to the crack. Additionally, the frequency characteristics of the sensors are crucial since they may mask the original frequency content of the wave. In this paper, the above factors are not thoroughly examined; the specimen size is quite small in order to exclude significant accumulation of scattering effects, as would occur in an actual size structure of several meters. On the other hand, the sensors are broadband in order to apply the least possible change in the content of the incoming signals. In any case the position of the sensors was fixed for all specimens and therefore, any change in the AE behavior

during the fracture experiment is attributed to the successive fracture modes. In the present study, the acoustic emission results of a long series of fracture tests in different types of concrete are discussed. The different types include plain concrete and steel fiber reinforced concrete with different fiber contents, shapes and coatings, as well as water to cement ratio, making a population of approximately 100 specimens. They were tested in four-point bending with concurrent monitoring of their AE activity. Each of these distinct material characteristics, i.e. shape of the fibers or existence of chemical coating, are reflected to certain discrepancies on the recorded AE behavior (Aggelis et al., 2010d,e). Nevertheless, the general behavior concerning the trends of AF and RA, as well as other AE parameters allows general conclusions for all materials independent of the mix and fiber parameters, based solely on the damage status; i.e. microcracking stage before the main crack formation, during the main fracture and afterwards as the damage is being continuously accumulated. The aim is to test the validity of a simple cracking mode characterization scheme based on specific AE parameters in laboratory. For this kind of AE parameter analysis a wide database is essential in order to increase the statistical importance of the conclusions. The present study includes approximately 100 specimens of different types of concrete which can be considered a significant population, compared to previous studies.

2. Experimental

Twenty five concrete mixtures were produced in total. Each mixture included four specimens. The specimens were prismatic, with dimensions $400 \times 100 \times 100$ mm. The water to cement ratio by mass (w/c) varied from 0.5 to 0.6 and 0.7. The maximum aggregate size was 10 mm and the steel fiber contents varied from 0% (plain concrete) to 0.5%, 1%, 1.5% and 2%. Three different basic shapes of steel fibers were used, namely undulated (wavy), fibers with hooked ends, and straight. The thickness of the fibers varied from 0.4, 0.5, 0.6 up to 0.7 mm and their lengths from 25 to 30 mm, resulting in aspect ratios from 40 to 62.5. The specimens were cured in water saturated with calcium hydroxide at $23 \pm 2\,°C$ for 28 days prior to testing. The specimens were subjected to four-point bending according to ASTM C1609/C 1609M-05 (Fig. 2) for toughness measurement. Details on the materials and mechanical testing can be found in Soulioti et al. (in press). As to AE monitoring, two AE broadband sensors (Pico, PAC) were attached to the bottom tensile side of the specimen (see again Fig. 2). The sensors were attached at the bottom surface in order to suitably monitor the initial weak micro-cracking which starts at the bottom side. Additionally, the bottom surface provides a free span of 300 mm to place the sensors while on the top, the loading points and the deflection measurement device which is placed in the middle reduce the free space. Roller bearing grease was used for acoustic coupling, while the sensors were secured by the use of tape during the experiment. The signals were recorded in a two-channel monitoring board PCI-2, PAC with a sampling rate of 5 MHz, pre-amplified
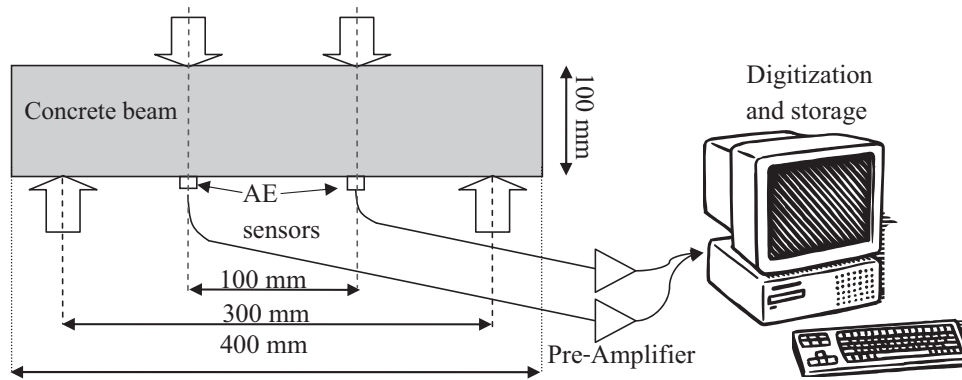
Fig. 2. Four-point bending setup and acoustic emission monitoring. AE behavior of concrete under bending.

by 40 dB, while in a previous study resonant sensors were used on a similar setup (Soulioti et al., 2009). The broadband sensors are considered appropriate because although their peak sensitivity is lower than resonant ones, the limited size of the specimens compensates for the wave attenuation. On the other hand, their wide frequency range enables more reliable acquisition of different sources closer to their original frequency.

In such materials, micro-cracking starts to develop initially, accompanied by a number of AE hits (see Fig. 3a). When the strength of the material is reached, a macroscopic crack is formed and a relatively large amount of vertical displacement is suddenly observed. At that moment a number of several tens of AE hits are recorded (see Fig. 3a). Thereafter, as the loading continues, the crack propagates to the top rupturing the rest of the concrete cross section while fibers bridging the crack are gradually being pulled out. At this stage, the AE hit rate is generally lower than the previous stage with decreasing tendency, mainly because most of the cross section has already been ruptured and the number of fibers to be pulled out are continuously reducing.

For plain concrete, the typical curve is similar until the main crack formation. At that moment the specimen is split into two parts and the experiment is terminated. It is reasonable that the AE activity recorded at the different stages exhibits distinct characteristics. Before the main crack, any hit originates from small events of matrix cracking. This cracking occurs due to the tensile load at the bottom of the specimen. At the stage of the main crack formation, which is the shortest in duration, a quite high rate of incoming AE signals is recorded (up to 100 hits/s). At that time the cracking events are more frequent and much stronger rupturing the brittle matrix with a visible crack, accompanied by several side cracks. Additionally, since the specimen starts to split into two main pieces, fiber pull out starts to occur, and is therefore responsible for a part of the recorded AE activity. These events resemble the shear type of failure due to the friction between the fibers and the surrounding concrete matrix. At the next stage (post-peak), the matrix continues to be slowly ruptured, and fibers to be pulled out until the termination of the experiment. The behavior of some typical AE parameters with time for the same experiment is depicted in Fig. 3b–d. The symbols stand for the value of the parameters while the line is the moving average of 30 recent hits. AF averages above 300 kHz during the tensile matrix cracking (Fig. 3b). This frequency corresponds to a major wavelength of approximately 10–15 mm (with a longitudinal wave velocity of 4000 m/s) which certainly exceeds the length of any micro-crack developed at this initial stage. At the moment of fracture several hits with low AF are observed, even AF close to zero, strongly decreasing the AF line, while thereafter, AF remains at levels lower than 200 kHz. It should be highlighted that the AE duration of each waveform (usually <1 ms), which is used for the calculation of AF as seen in Fig. 1, has no connection to
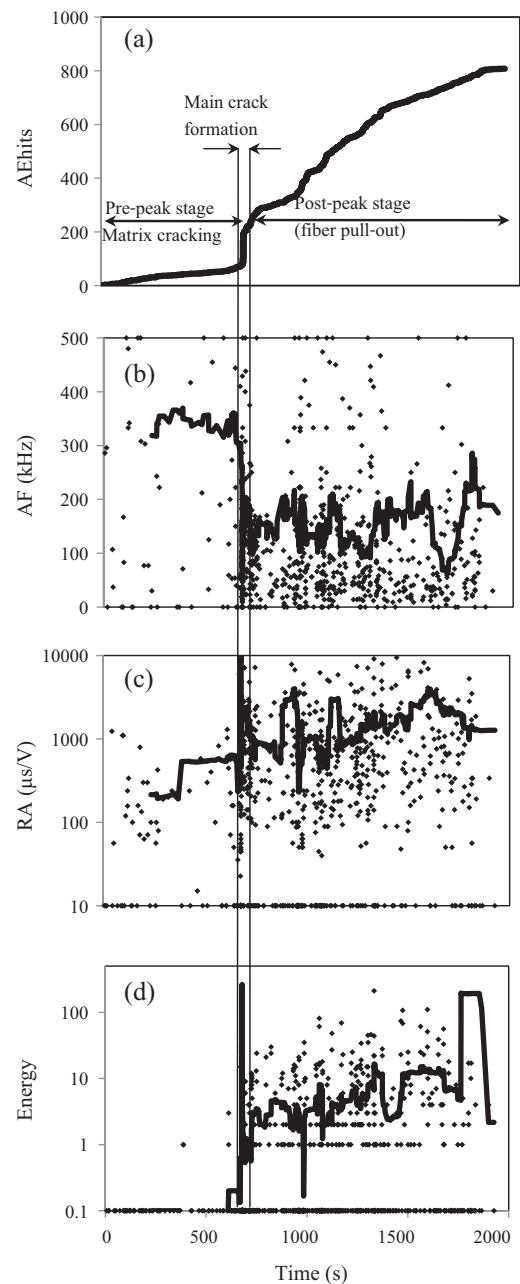

Fig. 3. Time history of (a) accumulated AE activity, (b) AF, (c) RA, and (d) AE energy for a steel fiber reinforced concrete specimen.

the duration of the whole macro-fracture stage (approximately 1 s), which includes several AE emissions. Concerning the RA history, the trend is inverse (Fig. 3c). Initially the typical values are below 500 μs/V. At the moment of fracture several hits with considerably higher RA are exhibited (even higher than 10 ms/V) and until the end of the experiment there is an increasing tendency as the damage is being accumulated. Additionally Fig. 3d shows the AE energy which exhibits its maximum at the moment of fracture while initially the energy of each AE hit was negligible. At the fiber pull out stage, the energy of the hits is increased by at least one order of magnitude compared to the initial. The above observations lead to some preliminary conclusions concerning the values of AE parameters corresponding to different modes of fracture. For the specific experiment included in Fig. 3 the AE hits are grouped based on the fracture stage. The average AF of the early cracking stage (of approximately 80 hits) is 291 kHz, while the 120 hits emitted during main fracture exhibited a severely decreased average AF of 117 kHz. At the last stage the average AF (of the recorded 600 hits) remained low, increasing slightly to 148 kHz. Concerning the other indices RA started with an average value of 486 μs/V, while at the moment of main fracture the average value was 4232 μs/V. Similarly the average energy increased by more than 60 times during the crack formation.

These discrepancies are large enough so that almost no overlap is observed even when AE data from different materials are grouped together. Fig. 4a shows the AF vs. RA for different fracture stages for all the 98 specimens. Each dot corresponds to the average of the whole population of hits of the specific stage for each specimen (i.e. before and during fracture). There is a very strong discrimination between the different stages based on these two AE parameters. Only a number of few dots are overlapping, allowing a robust classification by one straight line. When the AF of a signal is higher than 0.03*RA + 200, the crack can be securely classified to the tensile mode. Fig. 4b shows the corresponding correlation plot between AF and AE energy. The classification based on these two parameters is also strong, indicating that when the AF of a signal is higher than the ENE + 255 the crack is tensile. These graphs show that the combination of two of these parameters (AF, RA and ENE) can very well distinguish between different cracking modes in laboratory conditions. The fitted lines are indicative but not necessarily unique.

Another parameter showing high sensitivity to the fracture pattern is AE duration (DUR). Its correlation vs. energy is depicted in Fig. 4c, which shows a few more overlaps between micro-cracking and macro-fracture with pull out but still exhibits high classification potential.

The above results shed light in the fracture process enabling the characterization of the damage stage very reliably using only two or three parameters monitored nondestructively. It should be stated that in laboratory conditions, apart from the AE readings, other mechanical measurements are simultaneously applied, like load or displacement. Additionally, any macro-crack can be easily detected even by naked eye. The main benefit of such an approach with AE monitoring is that specific AE signatures are related to damage patterns; this is crucial for real size structures. In situ a crack of similar size will not result in visually detectable deflection and therefore, any assessment should be based solely on AE parameters. It is crucial therefore, that based on a few AE parameters the stage of damage for concrete materials can be estimated (e.g. initial stage, main fracture or post-peak).

It is worth to mention that in the AE field, due to the large population of signals, treatment is mostly statistical. The populations of data usually exhibit strong experimental scatter due to their different origins. This can be seen in Fig. 5, where the whole population of almost 300 points is included in three dimensional space for all fracture stages, as well as in Table 1. Under the
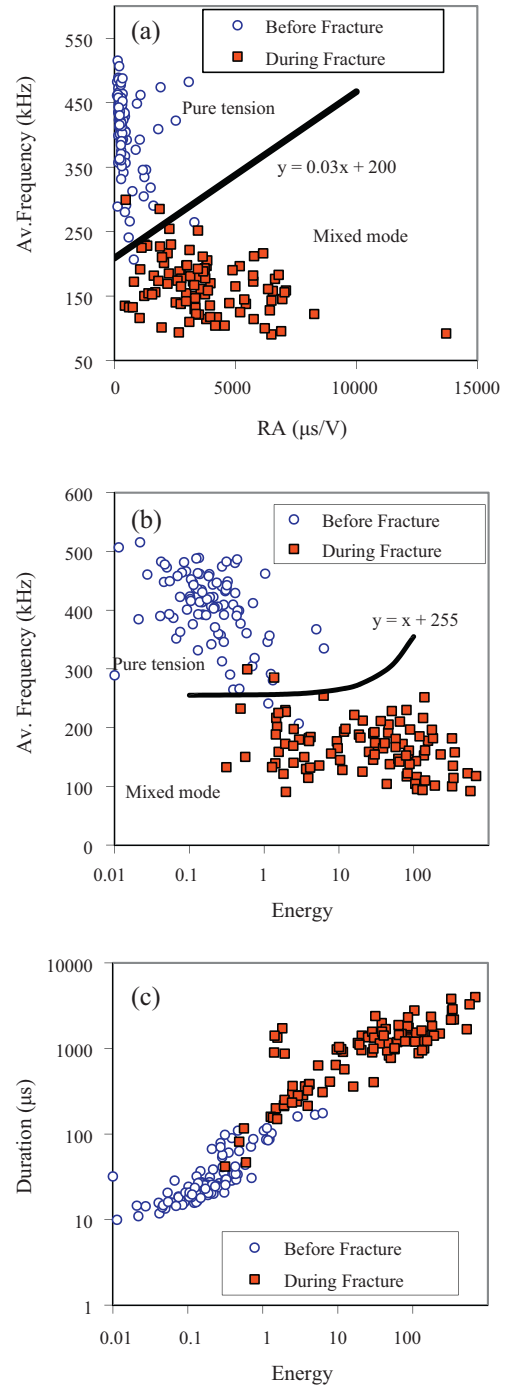

Fig. 4. Correlation plots between (a) AF and RA, (b) AF and AE energy, and (c) duration and AE energy.

Table 1
AE parameter ranges.

	AF (kHz)	RA (μs/V)	ENE	DUR (μs)
Micro-cracking				
Mean	405.3	500.3	0.41	39.3
COV[a]	15%	117%	208%	88%
Main fracture				
Mean	166.4	3679.0	78.71	1142.1
COV[a]	26%	57%	157%	71%
After main fracture				
Mean	311.8	1003.1	4.21	171.2
COV[a]	34%	91%	207%	100%

[a] Coefficient of variation, stands for the standard deviation divided by the average.
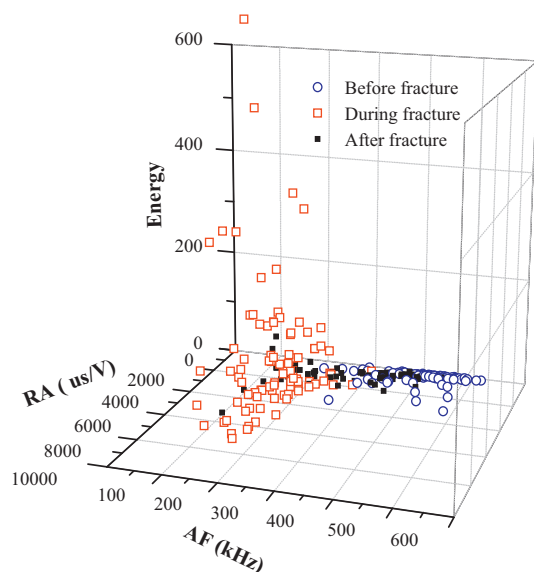
Fig. 5. Three dimensional correlation plot of the AE parameters for all fracture stages.

specific standard deviations (which in many cases exceed 100% of the average value), the fact that different populations of signals (before and during fracture) are totally separated shows that the specific AE parameters are really strong descriptors to be used in cracking mode characterization.

This is the first step in establishing a robust characterization scheme for the cracking mode in concrete at least in controlled laboratory conditions. Other aspects should be additionally examined. One important parameter is the inhomogeneity of concrete which imposes strong scattering on the propagating wave especially in cementitious materials (Punurai et al., 2007). Therefore, each signal, depending on the propagation distance from the source crack to the sensor, may be distorted and its parameters changed (Polyzos et al., 2010). In the specific case, the limited volume of the specimens allows to make conclusions without strong implications from inhomogeneity-induced distortion.

3. Conclusions

The present study discusses AE parameters to enable a simple classification scheme between different modes of fracture in concrete. A large population of specimens was fractured with concurrent monitoring of AE. Different AE parameters like the average frequency, RA and energy exhibit strong sensitivity to the fracture mode (tensile micro-cracking, macro-cracking or fiber pull out), showing that they can be included in a simple but reliable characterization scheme concerning the mode of damage in concrete. The usefulness of such a scheme is of paramount importance for studying the fracture behavior of materials, while the study should continue in the direction of application in real structures where large distances between sensors may pose additional difficulties in the signal interpretation.

Acknowledgement

References

Aggelis, D.G., Barkoula, N.M., Matikas, T.E., Paipetis, A.S., 2010c. Acoustic emission monitoring of degradation of cross ply laminates. J. Acoust. Soc. Am. 127 (6), EL246–EL251.

Aggelis, D.G., Matikas, T.E., Shiotani, T., 2010b. Advanced acoustic techniques for health monitoring of concrete structures. In: Kim, S.H., Ann, K.Y. (Eds.), The Song's Handbook of Concrete Durability. Middleton Publishing Inc., pp. 331–378.

Aggelis, D.G., Shiotani, T., Momoki, S., Hirama, A., 2009. Acoustic emission and ultrasound for damage characterization of concrete elements. ACI Mater. J. 106 (6), 509–514.

Aggelis, D.G., Shiotani, T., Terazawa, M., 2010a. Assessment of construction joint effect in full-scale concrete beams by acoustic emission activity. J. Eng. Mech. 136 (7), 906–912.

Aggelis, D.G., Soulioti, D.V., Sapouridis, N., Barkoula, N.M., Paipetis, A.S., Matikas, T.E., 2010d. Characterization of the damage process in fibre reinforced concrete using acoustic emission parameters. In: Proceedings of Structural Faults and Repair 2010 , Edinburgh, 15–17 June (in CD).

Aggelis, D.G., Soulioti, D.V., Sapouridis, N., Barkoula, N.M., Paipetis, A.S., Matikas, T.E., 2010e. Acoustic emission characterization of steel fibre reinforced concrete during bending. Proc. SPIE 7649, 764912, doi:10.1117/12.847396.

Carpinteri, A., Cardone, F., Lacidogna, G., 2010. Energy emissions from failure phenomena: mechanical, electromagnetic, nuclear. Exp. Mech. 50, 1235–1243.

Curtis, G.J., 1975. Acoustic emission energy relates to bond strength. Non-Destruct. Test. 8 (5), 249–257.

Grosse, C.U., Ohtsu, M., 2008. Acoustic Emission Testing. Springer, Heidelberg.

Kawasaki, Y., Tomoda, Y., Ohtsu, M., 2010. AE monitoring of corrosion process in cyclic wet–dry test. Constr. Build. Mater. 24, 2353–2357.

Kurz, J.H., Finck, F., Grosse, C.U., Reinhardt, H.W., 2006. Stress drop and stress redistribution in concrete quantified over time by the *b*-value analysis. Struct. Health Monit. 5, 69–81.

Matikas, T.E., 2008. Influence of material processing and interface on the fiber fragmentation process in titanium matrix composites. Compos. Interfaces 15 (4), 363–377.

Mindess, S., 2004. Acoustic emission methods. In: Malhotra, V.M., Carino, N.J. (Eds.), CRC Handbook of Nondestructive Testing of Concrete. CRC, Boca Raton, FL.

Ohno, K., Ohtsu, M., 2010. Crack classification in concrete based on acoustic emission. Constr. Build. Mater. 24 (12), 2339–2346.

Ohtsu, M., Tomoda, Y., 2007. Phenomenological model of corrosion process in reinforced concrete identified by acoustic emission. ACI Mater. J. 105 (2), 194–200.

Ohtsu (Chairman), M., 2010. Recommendations of RILEM Technical Committee 212-ACD: acoustic emission and related NDE techniques for crack detection and damage evaluation in concrete: 3. Test method for classification of active cracks in concrete structures by acoustic emission. Mater. Struct. 43 (9), 1187–1189.

Philippidis, T.P., Nikolaidis, V.N., Anastassopoulos, A.A., 1998. Damage characterization of carbon/carbon laminates using neural network techniques on AE signals. NDT&E Int. 31 (5), 329–340.

Philippidis, T.P., Nikolaidis, V.N., Kolaxis, J.G., 1999. Unsupervised Pattern Recognition Techniques for the Prediction of Composite Failure. J. Acoust. Emiss. 17 (1–2), 69–81.

Polyzos, D., Papacharalambopoulos, A., Shiotani, T., Aggelis, D.G., 2010. Dependence of AE parameters on the propagation distance. In: Wakayama, et al. (Eds.), Progress in Acoustic Emission XV, pp. 43–48.

Punurai, W., Jarzynski, J., Qu, J., Kurtis, K.E., Jacobs, L.J., 2007. Characterization of dissipation losses in cement paste with diffuse ultrasound. Mech. Res. Commun. 34, 289–294.

Shiotani, T., Aggelis, D.G., Makishima, O., 2009. Global monitoring of large concrete structures using acoustic emission and ultrasonic techniques: case study. J. Bridge Eng.-ASCE 14 (3), 188–192.

Shiotani, T., 2006. Evaluation of long-term stability for rock slope by means of acoustic emission technique. NDT&E Int. 39 (3), 217–228.

Soulioti, D., Barkoula, N.M., Paipetis, A., Matikas, T.E., Shiotani, T., Aggelis, D.G., 2009. Acoustic emission behavior of steel fibre reinforced concrete under bending. Constr. Build. Mater. 23, 3532–3536.

Soulioti, D.V., Barkoula, N.M., Paipetis, A., Matikas, T.E. Effects of fibre geometry and volume fraction on the flexural behaviour of steel-fibre reinforced concrete. Strain, in press.

Yuyama, S, Li, Z., Ito, Y., Arazoe, M., 1999. Quantitative analysis of fracture process in RC column foundation by moment tensor analysis of acoustic emission. Constr. Build. Mater. 13, 87–97.

Zhou, J.W., Xu, W.Y., Yang, X.G., 2010. A microcrack damage model for brittle rocks under uniaxial compression. Mech. Res. Commun. 37, 399–405.